β-decay rate of ^{79m}Se and its consequences for the s-process temperature

N. Klay and F. Käppeler
Institut für Kernphysik III, Kernforschungszentrum Karlsruhe, D-7500 Karlsruhe, Federal Republic of Germany
(Received 21 December 1987)

The branching ratio between internal electromagnetic transitions and β^- decays of the isomer ^{79m}Se was determined experimentally. Extremely clean samples of ^{78}Se were activated with thermal neutrons at a high-flux reactor. A mini-orange-Si (Li) detection system was used to measure β^- particles and conversion electrons immediately after neutron irradiation. For the β^- decay we obtain $\log ft = 4.70^{+0.10}_{-0.09}$. Our present result was used to recalculate the temperature dependence of the effective β^- half-life of ^{79}Se in the stellar interior. In combination with the half-life deduced from a quantitative branching analysis, we obtain a possible temperature range between 182 and 295 million degrees for the weak component of the s process.

I. INTRODUCTION

If the temperature in the interior of a star is sufficiently high, even excited nuclear states will be populated thermally. For the β^--unstable nucleus ^{79}Se this results in a change of the half-life because of the different $\log ft$ values for ground state and first excited states. The first excited state is a 3.9 min isomer at 96 keV which decays back by internal transitions but can also undergo allowed β^- decay. As the ground state decay is unique first forbidden, any excitation of the isomer results in an enhanced β^--decay rate for ^{79}Se. In the case of thermal excitation the half-life of ^{79}Se will therefore become a steep function of temperature.

On the other hand, a quantitative analysis of element synthesis by slow neutron capture (s process) can provide for the effective stellar half-life of ^{79}Se, which is considerably smaller than the terrestrial value. The possible range for the effective half-life was calculated from the observed element abundances and the neutron capture cross sections in the mass region $78 < A < 82$.[1,2]

The knowledge of the effective half-life offers the possibility to derive the temperature for the stellar site, where the s-process synthesis of ^{79}Se occurs. Previous work on this subject had to use theoretical estimates for the $\log ft$ values for excited states in ^{79}Se (Refs. 3-5) to calculate the β^- half-life as a function of temperature,[2,3] but the respective uncertainties were too large for a reliable analysis.

We have measured the $\log ft$ value for ^{79m}Se experimentally. The results of this measurement described in this paper enable the precise determination of the effective ^{79}Se half-life as a function of temperature. Consequently, we will give a rather narrow range of allowed temperatures for the site of the s process.

II. EXPERIMENTAL SETUP

The isomer ^{79m}Se decays with a 3.9 min half-life predominantly by internal transitions (Fig. 1), but also through a minor β^--branch. The life time of ^{79m}Se is long enough to allow for an activation experiment where ^{79m}Se is first produced via neutron capture on ^{78}Se and the beta decay is measured immediately afterwards.

The branching ratio $\lambda_\beta/\lambda_\gamma$, however, is expected to be only $\sim 10^{-4}$. Therefore the detection of the weak beta branch requires a high neutron flux to achieve sufficient activity, an extremely clean sample to avoid β^- backgrounds from activation of impurities, and a β^- spectrometer for suppression of the strong conversion lines from the competing internal transitions. These experimental conditions are discussed in the following paragraphs.

A. Sample preparation

Carbon was chosen as the most suitable backing material because it is conductive and will not be activated due to its low neutron capture cross section. Any impurities with high cross sections leading to products with half-lives comparable to ^{79m}Se had to be avoided. Some of the most critical impurities would be V, Cu, Al, and ^{80}Se.

Carbon of different origin has been tested for impurities via proton induced x-ray emission (PIXE). The only material of sufficient purity was found to be carbon for optical spectroscopy from Ringsdorff Werke GmbH, Bonn, Federal Republic of Germany (FRG). From a bar of their "RW-O" carbon thin disks of 0.1 mm thickness

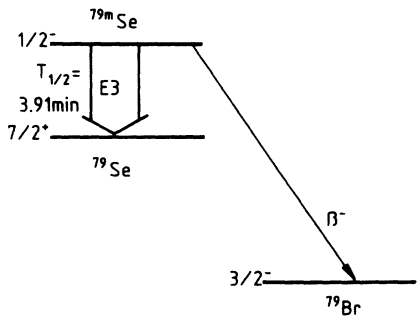

FIG. 1. Decay scheme of ^{79m}Se.

and 7 mm diameter were produced on a turning lathe. These disks were packed into small graphite cylinders and sent back to the supplier for a special recleaning procedure.

As a next step, ^{78}Se was implanted into the recleaned disks by a high resolution mass separator of the Kernforschungszentrum Karlsruhe GmbH cyclotron laboratory starting from 97.27% enriched ^{78}Se as source material. The final mass amounted to ~ 15 μg ^{78}Se on 6.7 mg graphite. In spite of this relatively large graphite mass, no metallic impurities have been detected either by PIXE measurements or by neutron activations with subsequent γ spectroscopy using a Ge (Li) detector. The latter test irradiations were carried out at the TRIGA reactor of the Krebsforschungszentrum, Heidelberg, FRG.

B. Spectrometer design

A spectrometer for detection of the ^{79m}Se β^- particles should have a high sensitivity but must also suppress the conversion electrons at 83 and 94 keV. A very high transmission over a wide energy range can be obtained by a mini-orange spectrometer consisting of a Si(Li) detector and a filter of permanent magnets.[6] We selected a geometry (Fig. 2) where the focusing property of the magnets led to an absolute transmission of 5.5% in the energy range from 100 keV up to the β^- endpoint of 256 keV. However, the standard design of this spectrometer was not optimized for a sharp cutoff at lower energies which is needed for suppression of the conversion lines. The reason for the rather poor low energy cutoff was found to be due to field inhomogeneities near the magnet surfaces. These were located carefully by means of a Hall probe and were shielded with a lead mask of 1 mm thickness (Fig. 2). With this improved arrangement direct transmission was almost eliminated below 100 keV (no electron lines below 100 keV), the remaining background being due to electron backscattering within the spectrometer. The intensity in the backscattering socket integrated between 45 keV and 94 keV corresponds to an absolute "transmission" of 0.09%, which is smaller by a factor of 60 compared with the mean transmission for β^- particles above 100 keV.

III. MEASUREMENTS

The neutron irradiations have been carried out at the high-flux reactor of the Institut Max von Laue-Paul Langevin, Grenoble. The ^{78}Se samples were irradiated for 2 and 4 min with a thermal neutron flux of 1.6×10^{14} cm^{-2}s^{-1}. A fast rabbit system connects the reactor with the Laboratoire à Moyen Activité of the adjacent Centre d'Etudes Nucléaires de Grenoble, where our spectrometer was installed. Including transport and unloading from the irradiation capsule, the sample was available ~ 2 min after the irradiation. Another 2 min were required for mounting the sample in the spectrometer and for pumping that part of the vacuum system which contains the sample holder. The valve which separates the Si(Li) detector was then opened to start the activity measurements at typically one half-life (3.9 min) after the activations. These were carried out in four steps: (1) The sequence was started with the β^- spectrum, which was recorded by a computer program in 1 min intervals for ~ 4 half-lives. In this way it was possible to follow the ^{79m}Se decay in time, an important consistency check for later analysis. (2) About 20 min after the end of irradiation the sample was removed from the spectrometer and placed 1 mm in front of a Ge(Li) detector in order to record the γ spectrum for investigation of backgrounds from activated impurities. (3) Meanwhile, the magnetic filter was removed from the β^- spectrometer and in a third step the conversion electrons were directly measured with the Si(Li) detector in order to determine the total ^{79m}Se activity. (4) Finally, the integrated longer-lived β^- background from the sample was measured with the mini-orange filter inserted again.

The resulting sum spectra for conversion electrons and β^- particles from one activation are shown in Fig. 3. The fact that the conversion lines do not show up in the β^- spectra taken with the mini-orange filter demonstrates that all low energy background is due to electron scattering at the walls. In total, we carried out 5 activations with 3 different samples whose results were combined in the final data analysis. In addition, background problems and systematic uncertainties were studied in a number of test activations.

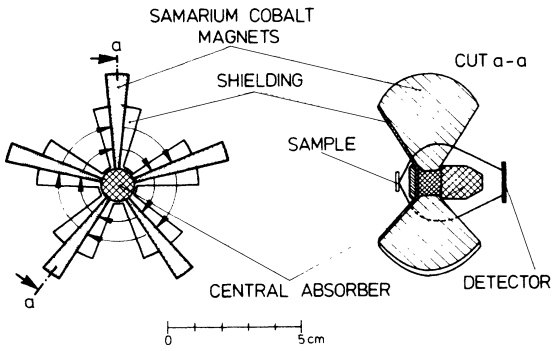

FIG. 2. Mini-orange spectrometer setup for suppression of conversion electrons below 96 keV. Idealized trajectories for electron energies of ~ 140 keV are indicated in the right part of the figure.

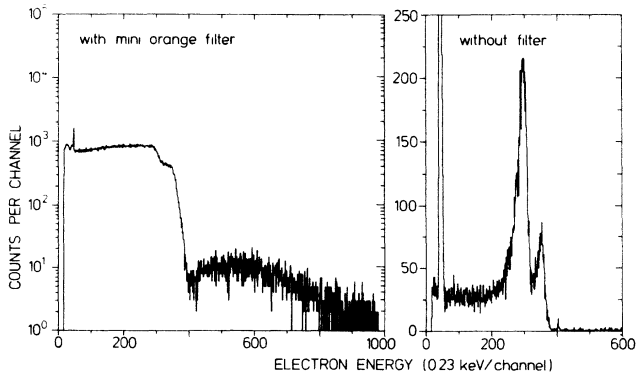

FIG. 3. Experimental spectra: Electrons from the beta decay of ^{79m}Se (left, counts beyond channel 400) and conversion electrons from the ground state transition (right).

An investigation of possible backgrounds from short lived β^- emitters was performed in two ways. First, the γ-ray spectrum of one of the samples was measured immediately after activation in the reactor instead of the β^- spectrum. The same ^{78}Se sample was then activated again, and the β^- spectrum was recorded with the Si(Li) detector but without the mini-orange filter. This measurement was started 3.1 min after the end of irradiation and covered the energy range up to 460 keV. The high energy part of the spectrum above the ^{79m}Se endpoint energy was used as a half-life test for the β^- background, while the low energy part with the intense conversion lines was used to determine the pileup rejection property of the electronics.

IV. DATA ANALYSIS AND BACKGROUND SUBTRACTION

The determination of the β^- countrate from ^{79m}Se has to be based on a detailed analysis of all background components. These originate from (a) activated impurities, (b) constant room background, and (c) pileup. The dominant contribution arises from activated impurities. In the Ge(Li) spectra γ rays from ^{41}Ar and ^{38}Cl could be detected, and it turned out that these two nuclides account for practically all of the longer-lived background. No other γ rays from the sample were detected besides a negligible contribution from ^{24}Na. The β^--activity ratio between ^{41}Ar and ^{38}Cl was determined from the γ intensities and the shapes of both β^- spectra were calculated theoretically. The ratio of partial β^- activities in the measured energy interval was then obtained by numerical integration. The experimentally measured integrated long-lived background could then be divided into its components. With the half-lives of ^{41}Ar (1.83 h) and ^{38}Cl (37.2 min), the background from activated impurities was determined as a function of time. It was found to be typically ~ 100 min^{-1} at the time when the activity measurement was started. The additional room background of (5 ± 1) min^{-1} was comparably small. Background due to pileup results from the remaining socket due to scattered conversion electrons. From the countrate between 50 and 96 keV the expected pileup rate above 100 keV was calculated using the known pair pulse resolution of the electronic system. For all activations, an upper limit of 15 min^{-1} additional pileup events can be quoted for the first 1 min spectrum. This contribution falls quadratically with time.

The sum over all background components has been subtracted from the measured total β^- countrate in the energy interval of interest between 100 and 230 keV. The remaining countrate is typically ~ 300 min^{-1} at the beginning of the measurement. Its decrease with time reproduces the 3.9 min total half-life of ^{79m}Se (Fig. 4), well within the uncertainties due to background subtraction. Hence it can be concluded that the subtraction of the long-lived background was correct.

However, the above procedure cannot exclude a contribution of another β^- emitter with a half-life of about 4 min. An example for such a contaminant is ^{52}V with a half-life of 3.75 min. Because of the high cross section of ^{51}V, our measurement is extremely sensitive to very small vanadium impurities. The average vanadium content of the high purity carbon used for sample preparation was specified to 0.01 ppm. For one sample backing that had not been recleaned after manufacturing in our workshop, we found a vanadium content of 0.08 ppm from the analysis of the gamma-ray spectrum, corresponding to a background rate of 130 min^{-1} in the first beta spectrum. Therefore this sample was rejected from further analysis.

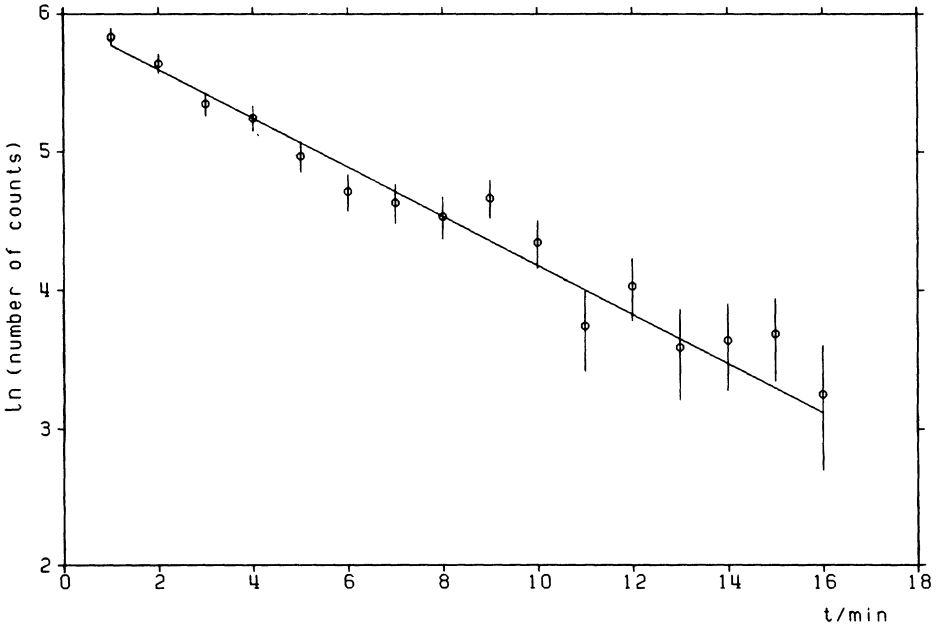

FIG. 4. Integral number of β^- counts (log scale) measured per 1 min step between 100 and 230 keV after subtraction of all background components as a function of time (linear scale). Note that the error bars give only the statistical error resulting from the total count rate. The straight line represents a least squares fit to the data for a fixed total half-life of 3.91 min.

For a recleaned sample backing we can place an upper limit of 0.4 ppb from the detection sensitivity in the Ge(Li) spectrum measured 5.4 min after neutron irradiation. The resulting upper limit for β^- background from ^{52}V is 0.7 min^{-1}.

A more general exclusion of other short-lived background emitters can be obtained from the measured beta spectrum above the endpoint energy of ^{79m}Se. A $Z<82$ nuclide which undergoes allowed beta decay with $t_{1/2}=4$ min must have an endpoint energy greater than 1 MeV, otherwise the statistical factor would be too low. Therefore any short-lived beta emitter contributes significantly to the measured beta spectrum above the endpoint energy of ^{79m}Se. The time dependence of the countrate measured in the energy interval from 260 to 460 keV is shown in Fig. 5 (symbols with error bars). There is no evidence for a component with a 4 min half-life, whereas the decay of ^{38}Cl and ^{41}Ar is reproduced very well (solid line). If an additional component with $t_{1/2}=4$ min and an intensity of 20% of the initial countrate is assumed artificially, the fit to the measured background would be already bad. The influence of such a component on the spectrum region of interest between 100 and 230 keV is maximal for a nuclide of low endpoint energy and high Z. An upper limit for the respective correction can therefore be derived from the spectral shape of ^{206}Tl with $E_0=1.53$ MeV and $Z=81$. This shape has been compared with that of ^{41}Ar ($E_0=1.2$ MeV), the most dominant background component. It is found that for equal intensity in the high energy window both nuclides contribute about equally. A 20% admixture of a short lived component in the high energy window will therefore transform in a contribution of 20% of the β^- background in the ^{79m}Se spectra. Such an undetected short lived β^- background would result in a ^{79m}Se countrate overestimated by (7 ± 1)%. Although there is no evidence for such a component in the high energy data, a 7% uncertainty is assumed as an upper limit.

In conclusion, we have demonstrated that the events shown in Fig. 3 indeed result from the beta-decay of ^{79m}Se. The various steps of data analysis are listed for one of the samples in Table I. A summary of all measured β^- counts and backgrounds for the five activations is given in Table II.

The net beta count rates have to be normalized to the electromagnetic transition rates that were obtained via the conversion lines measured without mini orange filter. This has the advantage that various efficiency factors cancel out by combining the two electron count rates instead of using the gamma-ray transitions directly. The peak contents of $K+L+M$ lines, which were not completely resolved, was calculated by subtracting a constant backscattering component as determined from the left of the average peak center.

All measured count rates were normalized for $t=3.91$ min $\hat{=}t_{1/2}$ (^{79m}Se) after neutron irradiation. The results as well as the ratios of conversion electrons and β^- particles N_e/N_{β^-} are given in Table III. The mean ratio averaged over all activations is $N_e/N_{\beta^-}=856\pm40$ excluding the upper limit for a short lived background. Taking this into account one finally obtains

$$N_e/N_{\beta^-}=856^{+100}_{-40}\ .$$

V. EFFICIENCY CALIBRATION

For the calculation of the branching ratio $\lambda_\gamma/\lambda_\beta$ from the β^- and conversion electron count rates, one has to determine the ratio between the efficiency of the mini-orange detector system for β^- particles from the ^{79m}Se decay and the Si(Li)-detector efficiency for conversion electrons. In the investigated energy interval from 100 to 230 keV the β^- spectrum of ^{79m}Se can be well approximated by the spectrum of a ^{45}Ca source, which has an endpoint energy comparable with that of ^{79m}Se. A difference of the spectral shapes appears mainly at low energies due to the different Fermi functions, whereas the

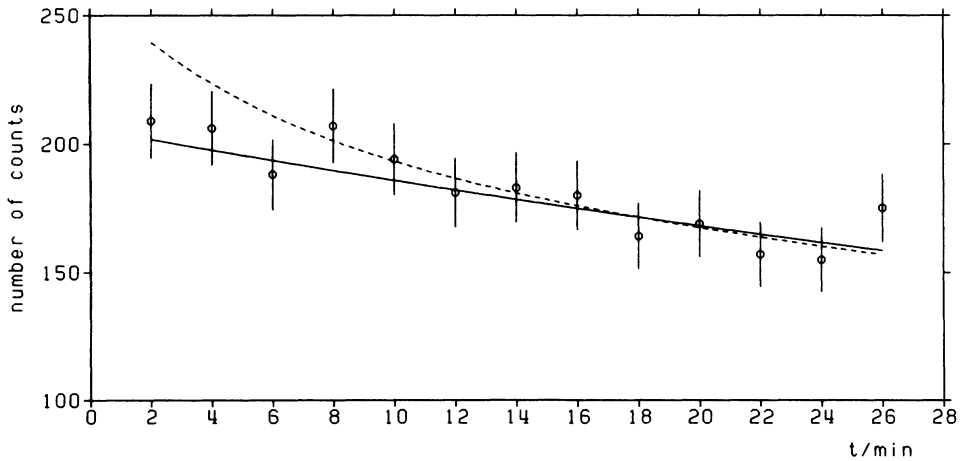

FIG. 5. Integral number of β^- counts measured in 2 min steps between 260 and 460 keV as a function of time for the test activation without the mini-orange filter. The start of this measurement ($t=0$) was 3.1 min after the activation. The data are fitted for $t>10$ min and two cases are indicated: (i) the solid line refers to an admixture of ^{41}Ar and ^{38}Cl as determined from the Ge(Li) spectra and (ii) the dashed line assumes an additional short lived background component.

TABLE I. Details from the analysis of the β^- count rate for one activation. The measurement was started 4.134 min after the end of irradiation. Background subtraction was performed for the β^- countrates $N(^{41}\mathrm{Ar})=77$ min and $N(^{38}\mathrm{Cl})=30$ min at the end of irradiation and a constant room background of 5 min^{-1}. For each 1 min step of the measurement the number of β^- counts after complete background subtraction is compared with a fit function for an exponential decay with a 3.91 min half-life. The same results are plotted in Fig. 4.

			Background components							
t/min	Number of counts	Statistical error	^{41}Ar	^{38}Cl	Pileup	Total background	Counts from ^{79m}Se	Fit function	Fit minus measurement	χ^2
1	460	21.4	75.0	27.8	10.1	117.9	342.1	322.1	−20.0	0.87
2	396	19.9	74.5	27.3	7.1	113.9	282.1	269.8	−12.3	0.38
3	321	17.9	74.1	26.8	5.0	110.8	210.2	226.0	15.8	0.77
4	298	17.3	73.6	26.3	3.5	108.4	189.6	189.2	−0.4	0.00
5	250	15.8	73.1	25.8	2.4	106.4	143.6	158.5	14.9	0.89
6	216	14.7	72.7	25.3	1.7	104.7	111.3	132.8	21.5	2.13
7	206	14.4	72.2	24.8	1.2	103.3	102.7	111.2	8.5	0.35
8	195	14.0	71.8	24.4	0.8	102.0	93.0	93.1	0.1	0.00
9	207	14.4	71.3	23.9	0.6	100.8	106.2	78.0	−28.2	3.83
10	177	13.3	70.9	23.5	0.4	99.8	77.2	65.3	−11.9	0.80
11	141	11.9	70.4	23.1	0.3	98.8	42.2	54.7	12.5	1.11
12	154	12.4	70.0	22.6	0.2	97.8	56.2	45.8	−10.4	0.70
13	133	11.5	69.5	22.2	0.1	96.9	36.1	38.4	2.3	0.04
14	134	11.6	69.1	21.8	0.1	96.0	38.0	32.1	−5.8	0.26
15	135	11.6	68.7	21.4	0.1	95.1	39.9	26.9	−12.9	1.24
16	120	11.0	68.2	21.0	0.0	94.3	25.7	22.6	−3.2	0.08

TABLE II. Results of the β^- spectra.

Activation No.	Sample No.	Irradiation time (min)	Number of counts in the first β^- spectrum over 1 min: Total	^{41}Ar	^{38}Cl	Pileup	^{79m}Se (fit of all spectra)
5	7	2	247	49	14		164±16
9	9	4	414	78	32	12	264±20
10	7	4	413	73	21	9	311±30
11	8	4	460	75	28	10	322±20
12	9	4	366	65	26	6	257±20

measured energy interval is not affected.

Therefore the efficiency of the mini-orange detector system for ^{79m}Se can be determined by means of a calibrated ^{45}Ca source with a correction for the different spectral shapes,

$$\varepsilon_\beta(\mathrm{Se})=\varepsilon_\beta(\mathrm{Ca})\frac{P(\mathrm{Se})}{P(\mathrm{Ca})} , \tag{5.1}$$

where ε_β is the absolute efficiency for β^- decays from Se and Ca, respectively, and P denotes the spectrum fraction in the measured energy window,

$$P=\frac{\int_{100\ \mathrm{keV}}^{230\ \mathrm{keV}} N(E)dE}{\int_0^{E_0} N(E)dE} . \tag{5.2}$$

The beta spectrum $N(E)$ is given by

$$N(E)dE=\varepsilon(\varepsilon^2-1)^{1/2}\frac{(\varepsilon_0-\varepsilon)^2}{m_0c^2}F(Z,E)dE , \tag{5.3}$$

with

$$\varepsilon_{(0)}=\frac{E_{(0)}}{m_0c^2}+1 , \tag{5.4}$$

where m_0c^2 denotes the electron mass in energy units and $F(Z,E)$ is the Fermi function. The results of a numerical integration using tabulated values for $F(Z,E)$ (Ref. 7) are

$$P(\mathrm{Se})=0.273\pm0.005 ,$$

$$P(\mathrm{Ca})=0.316\pm0.002 .$$

The quoted uncertainties correspond to the respective uncertainties in the β^--endpoint energies E_0. For ^{79}Se the most recent value of the nuclear mass tables[10] for the ground state decay and the well known excitation energy result in $E_0=(246.6\pm2.2)$ keV. For ^{45}Ca the adopted value is $E_0=(256.5\pm1.0)$ keV.

A suitable source for determining the conversion electron efficiency is ^{109}Cd, which emits L,M,N lines with a mean energy of 84 keV. We used the sum peak from these unresolved lines for calibration of our Si(Li) detector. The peak content was determined in a similar way as for the ^{79m}Se lines. The efficiency ε_{gs} for the ground state transition of ^{79m}Se is calculated from

$$\varepsilon_{gs}(\mathrm{Se})=\varepsilon_e 0.905(4) , \tag{5.5}$$

$$\varepsilon_e=\frac{N_e(\mathrm{Cd})}{A(\mathrm{Cd})0.538(2)} . \tag{5.6}$$

Here ε_e denotes the detector efficiency for 84 keV electrons. A(Cd) is the source activity of ^{109}Cd and N_e(Cd) is the measured count rate from L,M,N-conversion electrons. The factor 0.538(2) refers to the fraction of emitted L,M,N electrons per decay of ^{109}Cd, whereas the factor 0.905(4) in Eq. (5.5) is the conversion coefficient for the transition of ^{79m}Se to the ground state.[8]

Both the efficiency for conversion electrons and for β^- particles were not constant during the ^{79m}Se measurement. This is due to a dead layer which is trapped on the surface of the cooled Si(Li) detector. The dead layer results from the short evacuation times after mounting the samples and increased with each activation. This effect could be quantified via the energy loss of the conversion electrons.

For the later calibration measurements the detector

TABLE III. Results for the conversion electron spectra and a summary of count rates normalized to 3.91 min after neutron irradiation.

Activation No.	Start of first β^- spectrum (min)	Normalized ^{79m}Se β^- count rate (min^{-1})	Start of conversion electron measurement (min)	Peak content in the first 1 min spectrum	Normalized count rate of conversion electrons N_e (sec^{-1})	N_e/N_{β^-}
5	4.850	214±21	32.900	1065±15	3300±50	926±104
9	4.312	309±23	31.504	1726±45	4180±110	812±82
10	4.625	385±35	30.678	2554±65	5340±140	833±88
11	4.134	367±35	29.813	2892±65	5190±120	849±100
12	4.383	305±24	27.360	3862±70	4490±80	883±85

surface was recleaned by heating it to room temperature and by pumping it for several days. Then the measurements with the ^{45}Ca and ^{109}Cd sources were performed alternatively with short evacuation times in between. For every pair of β^-- and subsequent conversion electron measurement, the efficiencies ε_β(Ca) and ε_e were determined as a function of the conversion electron peak position. Within the range of energy losses observed during the selenium activations both efficiencies decreased by $\sim$20%. However, the efficiency ratio $\varepsilon_\beta(\mathrm{Ca})/\varepsilon_e = 2.25$ was found to be independent of the energy loss within $\pm$2%.

Other contributions to the systematic uncertainty of $\varepsilon_\beta/\varepsilon_e$ arise from the source activities and from the size of the β^- source. The latter uncertainty is due to the narrow geometry of the mini-orange spectrometer. As the diameter of the ^{78}Se layer was 3 mm, the diameters of the ^{45}Ca sources were chosen between 2 and 4 mm, resulting in a variation in transmission by $\pm$6.4%. A summary of all uncertainties is given in Table IV, the total uncertainties in $\varepsilon_\beta/\varepsilon_e$ being 17% for the described calibration procedure.

Because the largest uncertainty of the preceding calibration arises from the absolute source activities, an additional relative calibration was performed. Analogous to the selenium activations, a ^{45}Ca source was measured with mini-orange filter and afterwards with the filter removed just as the ^{79m}Se samples. The experimental value for the count rate ratio in the energy interval of interest was

$$T_r = \frac{\text{count rate with miniorange}}{\text{count rate without miniorange}} = 5.45 \pm 0.35 \ .$$

This result is the average obtained with samples of 3 ± 1 mm diameter. It determines directly the focusing effect of the magnetic filter. With this value, the final efficiency factor can be obtained by

$$\frac{\varepsilon_\beta(\mathrm{Ca})}{\varepsilon_e} = T_r \frac{\varepsilon_\beta^*}{\varepsilon_e} \ , \tag{5.7}$$

where ε_β^* denotes the efficiency for β^- particles from the ^{45}Ca decay as determined without the mini-orange filter. This efficiency can be calculated if the response function of the detector is well known. For the following calculation, a response function given by a narrow full energy peak and an energy independent back scattering socket[9] will be used. The count-rate ratio g between backscattering socket and full energy peak has been determined with line sources. It remains constant in the energy region of interest at the rather high value $g = 0.80 \pm 0.04$, which is mainly due to backscattering at the walls of the vacuum chamber. Backscattered β^- particles result in a distorted spectral shape and enhance the detected count rate. The number of additionally detected particles per energy unit can be expressed by

$$R(E)dE = \left[g \int_E^{E_0} \frac{N(E')}{E'} dE' \right] dE \ . \tag{5.8}$$

In the calculation of $\varepsilon_\beta^*/\varepsilon_e$ the factors for solid angle and count rate losses due to backscattering at the Si(Li) surface cancel out. Therefore, only the fraction of detected β^- particles corrected for backscattering appears in this ratio,

$$\frac{\varepsilon_\beta^*}{\varepsilon_e} = \frac{\int_{100\ \mathrm{keV}}^{230\ \mathrm{keV}} [N(E)+R(E)]dE}{\int_0^{E_0} N(E)dE} \ . \tag{5.9}$$

The result of a numerical integration, again using Eq. (5.3) for $N(E)$, is

$$\frac{\varepsilon_\beta^*}{\varepsilon_e} = 0.386 \ .$$

Note that the only experimental quantity included here is the backscattering ratio g. The error in g only results in a 1% error in $\varepsilon_\beta^*/\varepsilon_e$ because the measured high energy part of the spectrum is not too strongly affected by backscattering.

A comparison of the theoretically deduced spectral shape with a measured spectrum of ^{45}Ca (Fig. 6) shows good agreement for the β^- energies used in the evaluation. Because of the uncertainty in the endpoint energy of $\pm$2 keV and a possible energy loss of 2 keV in the measured spectrum, an additional uncertainty of 5% in $\varepsilon_\beta^*/\varepsilon_e$ must be considered.

The result for this part of the calibration is obtained by including the factor T_r,

$$\frac{\varepsilon_\beta(\mathrm{Ca})}{\varepsilon_e} = 2.10 \pm 12.4\% \ .$$

It should be mentioned that this value was derived without corrections for energy loss. This is justified because it was already shown that the energy loss during the selenium activations did not affect the ratio $\varepsilon_\beta/\varepsilon_e$.

Therefore a direct comparison with the calibration result via sources of known activity can be made. Both results are independent except for the common uncertainty in the transmission of the mini-orange filter. Excluding this 6.4% error, the two values 2.25 ± 0.23 and 2.10 ± 0.13 are consistent within the uncertainties. The unweighted average including all uncertainties will be used in the further analysis,

$$\frac{\varepsilon_\beta(\mathrm{Ca})}{\varepsilon_e} = 2.18 \pm 0.25 \ .$$

The efficiency factor for ^{79m}Se is obtained via Eqs. (5.6) and (5.1),

$$\frac{\varepsilon_\beta(\mathrm{Se})}{\varepsilon_{gs}} = \frac{P(\mathrm{Se})}{P(\mathrm{Ca})} (2.41 \pm 0.28) = 2.08 \pm 0.30 \ .$$

TABLE IV. Contributions to the total uncertainty in the efficiency factor $\varepsilon_e/\varepsilon_\beta$ for the calibration with sources of known activity.

Transmission of the mini-orange filter	6.4%
Energy loss	$\sim$2%
^{45}Ca source activity	5.4%
^{109}Cd source activity	3%

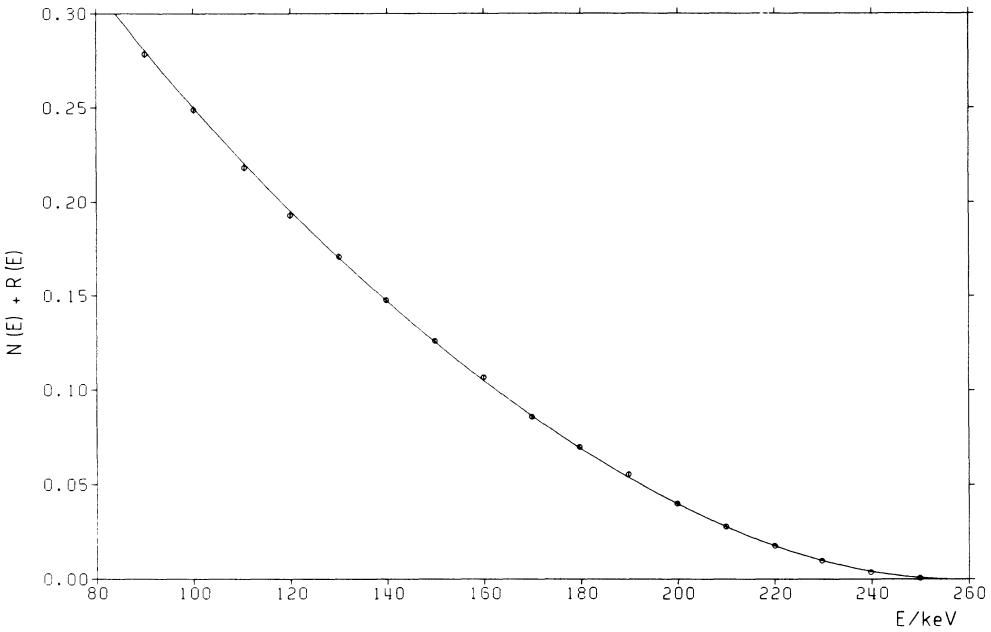

FIG. 6. Theoretically deduced spectral shape (solid line) as given by Eqs. (5.3) and (5.8) in comparison with the measured β^- count rate per energy interval (circles) normalized at 140 keV.

VI. DETERMINATION OF THE LOGft VALUE

From the results of the activations and the efficiency calibration the branching ratio between internal electromagnetic transitions and β^- decays can be determined,

$$\frac{\lambda_\gamma}{\lambda_\beta}=\frac{N_e}{N_\beta}\frac{\varepsilon_\beta(\mathrm{Se})}{\varepsilon_{gs}} . \tag{6.1}$$

The branching ratio for ^{79m}Se is therefore

$$\frac{\lambda_\gamma}{\lambda_\beta}=1780^{+560}_{-310} .$$

All uncertainties discussed above are considered and are conservatively combined by a linear summation. As λ_γ is well known, the partial half-life of ^{79m}Se against β^- decay can be derived without additional uncertainties. This partial β^- half-life is the key for a quantitative treatment of the temperature dependence of the effective half-life of ^{79}Se. Nevertheless, it is more usual to quote the logft value for the β^- decay. The transformation into this quantity is very sensitive to the β^- endpoint energy E_0. For our calculation of the statistical factor, the value $E_0=246.6$ keV (Ref. 10) was used. The final result is

$$\log ft=4.70^{+0.10}_{-0.09} .$$

VII. ASTROPHYSICAL CONSEQUENCES

With our present result for the logft value the temperature dependence of the effective stellar half-life of ^{79}Se can be calculated. Yokoi and Takahashi[3] elaborated a formalism which also accounts for the enhancement of the decay rate by β^- decay into ionized states. This so-called bound state decay contributes $\sim 25\%$ to the enhancement of the decay rate. Inserting the experimentally possible range of logft values, we obtain the error band for the effective half-life given in Fig. 7. A possible uncertainty of the assumed electron density of 10^{27} cm^{-3} has a minor influence on the result.

In Fig. 7 a remaining ambiguity in the ground state half-life is also indicated. For this quantity only an upper limit of 65 000 y is known experimentally.[8] For estimating a lower limit, log$ft=8.5$ was assumed as it is usually expected for unique first forbidden transitions. This value corresponds to a ground state half-life of 1700 y, considerably lower than the experimental upper limit. Nevertheless, the effective stellar half-life at temperatures above 200 million degrees is not changed by the assumed lower limit for the ground state half-life. This leads to the rather strange consequence that, at present, we know the stellar life time of ^{79}Se at a fixed temperature much better than its terrestrial one.

The real stellar β^- half-life of ^{79}Se can be derived in a completely independent way from the systematics of element synthesis by slow neutron capture (s process). This process, which contributes significantly to the synthesis of elements heavier than ^{56}Fe, is characterized by the product of neutron capture cross section σ and solar abundance N of each involved nuclide. This product is found to be a smooth function of mass number A.

The function $\sigma N(A)$ is reproduced very well by the classical model, which assumes that a fraction G of the natural iron abundance was irradiated by an exponential distribution of neutron exposures

$$\rho(\tau)=\frac{G}{\tau_0}\exp(-\tau/\tau_0) \tag{7.1}$$

that is characterized by a mean neutron exposure τ_0. For

a reproduction of the *s*-only isotopes along the *s*-process path, two different components need to be considered. The main component, with $\tau_0 = 0.30\ \text{mb}^{-1}$, allows for the production of the *s* abundances in the mass range $A > 100$, while the weak component with $\tau_0 = 0.06\ \text{mb}^{-1}$ is required to reproduce the steep slope of the $\sigma N(A)$ curve towards the iron group nuclides.[11] The smooth $\sigma N(A)$ curve shows strong deviations for those nuclides, where the β^- half-life is of the same order as the mean neutron capture time. At these so called branching points, competition between β^- decay and neutron capture causes the $\sigma N(A)$ curve to split. If the β^- half-life is independent of temperature the neutron capture rate can be derived from such a branching point. However, some branchings like that at ^{79}Se depend on temperature as well and can therefore be used as thermometers for the *s* process.

In the considered mass region both main and weak component contribute to nucleosynthesis. The main component can be adjusted in the mass region $A > 100$.[11] Then the parameters for the weak component are determined by the remaining contribution in the mass region $56 < A < 100$. By an analysis similar to that of Walter *et al.*[1,2] we have first investigated the ^{85}Kr branching to derive the neutron density and then evaluated the effective β^- half-life of ^{79}Se in the next step.

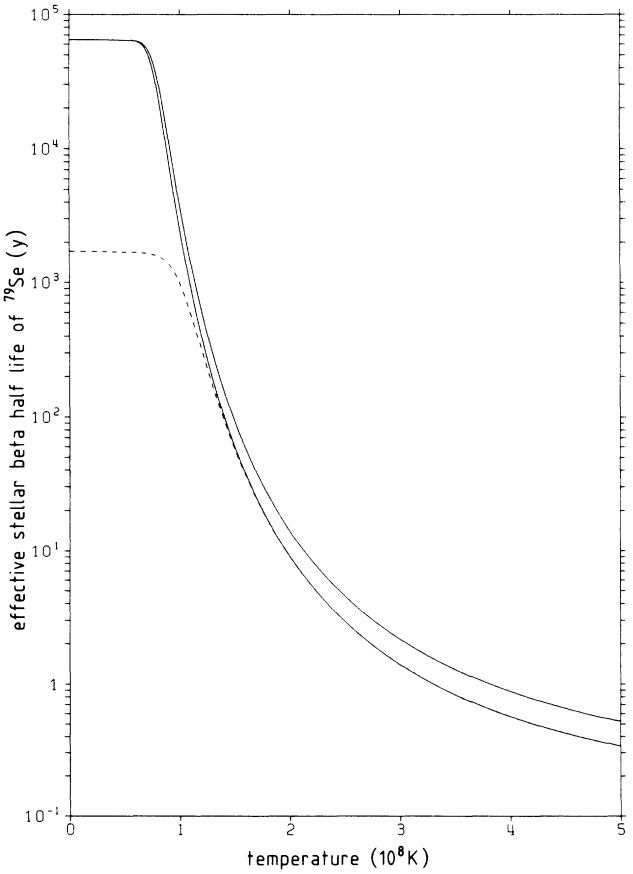

FIG. 7. Stellar half-life of ^{79}Se as a function of temperature. The error band reflects the uncertainty of our measurement. The dashed line refers to $\log ft = 8.5$ for the ground state decay.

The current analysis was performed with the recommended neutron capture cross sections from the compilation of Bao and Käppeler[12] with some renormalizations based on a recent, precise measurement of the ^{197}Au cross section,[13] which was often used as a standard. Only for ^{87}Rb the recommended value was not adopted because of inconsistencies with recent results.[14] Consequently, ^{87}Rb was not used for normalization of the *s*-process flow and hence does not influence the possible range of neutron densities derived from the ^{85}Kr branching.

The contribution of the main component was calculated for the physical conditions $kT = 23$ keV and $n_n = 1.3\ 10^8\ \text{cm}^{-3}$. The parameters G and τ_0 for the neutron exposure distribution were determined by a least square fit to empirical data for $A \geq 100$ using the code SPEED CLAS.[15] All these parameters were kept fixed for further analysis. The corresponding parameters for the weak component were fitted as to reproduce the experimental σN values of the *s*-only or *s*-dominated nuclides from ^{58}Fe to ^{88}Sr. The resulting range for the neutron density is

$$0.8 \leq n_n / 10^8\ \text{cm}^{-3} \leq 1.9\ .$$

The upper and lower limits were chosen as to avoid overproduction of the corresponding nuclide from the isobaric pair ^{86}Kr and ^{86}Sr.

For the ^{79}Se branching, the empirical σN values of the two *s*-only isotopes ^{80}Kr and ^{82}Kr must be reproduced by the $\sigma N(A)$ curve. After this function is normalized to ^{82}Kr, the limits for the stellar beta decay rate of ^{79}Se have to avoid over- or underproduction of ^{80}Kr for a given neutron capture rate (i.e., neutron density).

The resulting limits for the beta half-life which consider the whole range of possible neutron densities are

$$2.3y \leq T_{1/2}(\beta) \leq 16y\ .$$

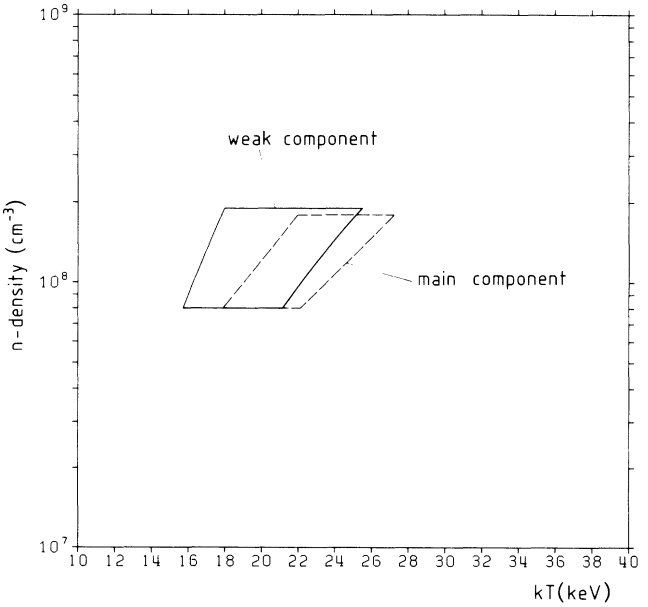

FIG. 8. Physical conditions for the two components of the *s* process.

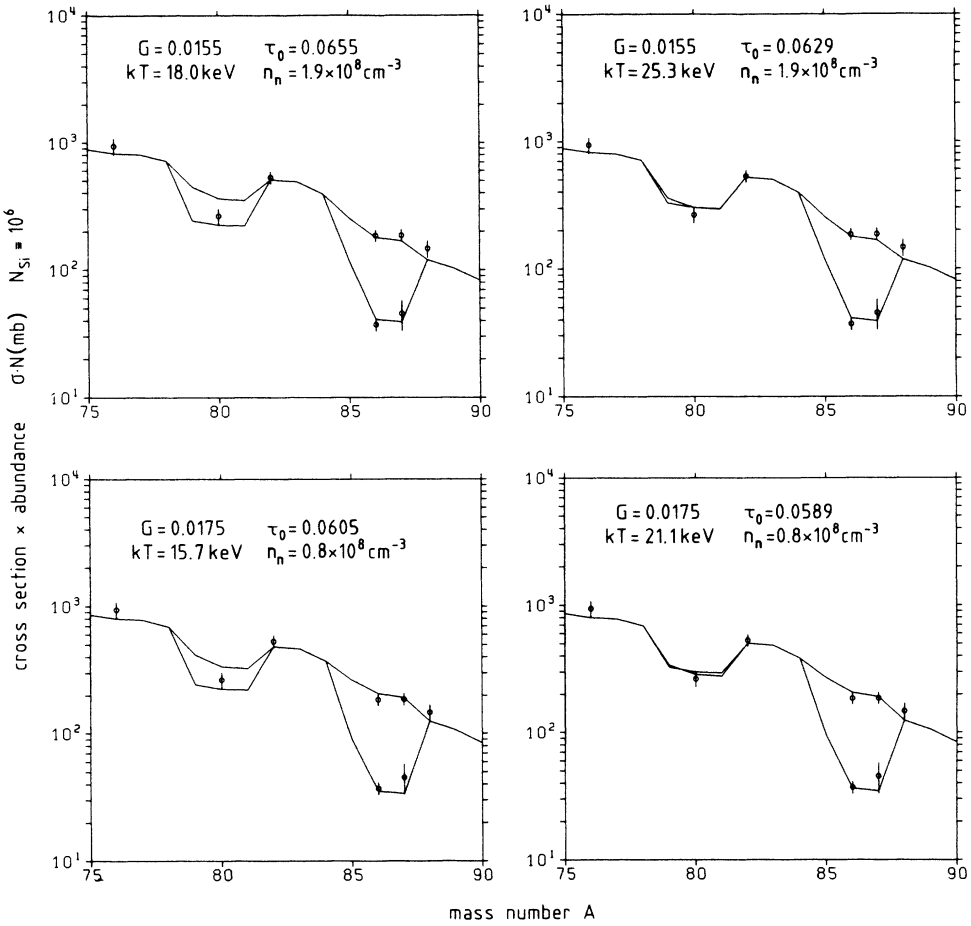

FIG. 9. $\sigma N(A)$ curves corresponding to the extreme combinations of temperature and neutron density for the weak component given in Fig. 8. The parameters for the weak component are indicated at the top of each plot.

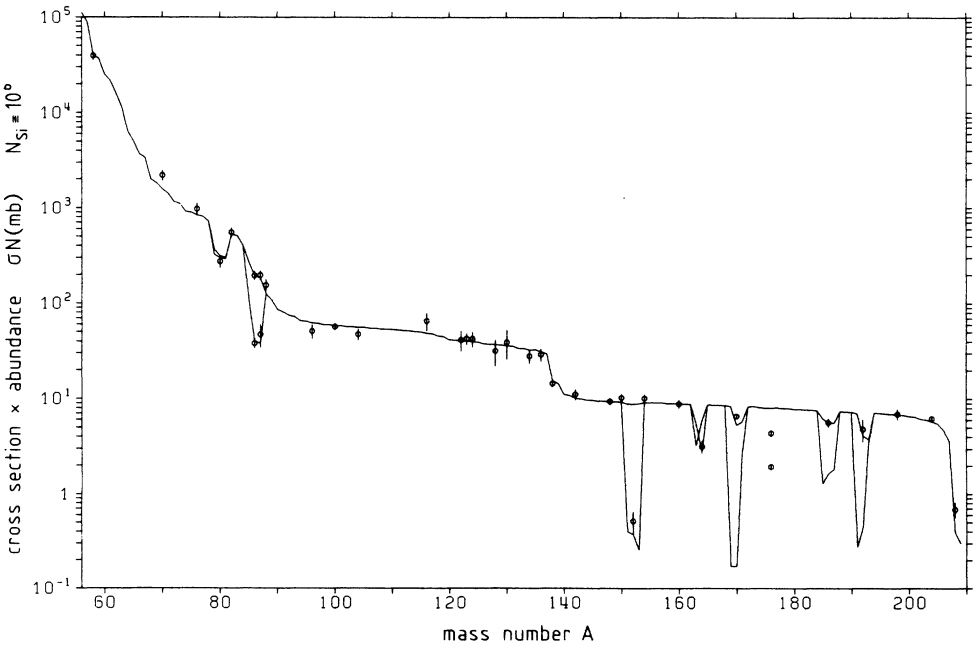

FIG. 10. Characteristic $\sigma N(A)$ function for the classical s process model with two components. The solid line represents a fit to the empirical data of s-only and s-dominant nuclides (symbols with error bars). For both the weak and main component a temperature $kT = 21.5$ keV and a neutron density $n_n = 1.3 \times 10^8$ cm^{-3} was assumed.

TABLE V. Numerical values for the half-life of ^{79}Se as a function of temperature. The values are calculated with $\log ft = 4.70$, corresponding to the center of the error band of Fig. 7. The unit of T is 10^8 K.

Electron density (cm^{-3})	Half-life (yr)					
	$T=1.0$	1.5	2.0	2.5	3.0	4.0
0.3×10^{27}	2823	69.7	10.8	3.53	1.69	0.689
1.0×10^{27}	3066	73.1	11.1	3.61	1.72	0.700
3.0×10^{27}	3176	74.5	11.9	3.85	1.81	0.720

In spite of this large uncertainty we can transform these limits into a rather narrow temperature range because of the steep function in Fig. 7. This essentially requires that the temperature dependence of the ^{79}Se half-life is precisely known, thus underlining the necessity of the present experimental determination. Hence one reads from Fig. 7 the temperature for the stellar site of the weak s-process component to range between 182 and 295 million degrees.

The related uncertainty is mainly due to the uncertainty for the effective stellar half-life deduced from the σN systematics which can only be reduced by improved cross section measurements. The present experimental uncertainty for the $\log ft$ value of ^{79m}Se contributes only to a small extent to the width of the temperature range: For $\log ft \equiv 4.70$ we obtain a temperature range between 188 and 278 million degrees.

In order to compare the physical conditions for the weak s-process component with those derived previously for the main component,[11] the correlation between neutron density and temperature is given more explicitly in Fig. 8. The area inside the solid lines corresponds to the possible values for neutron density n_n and temperature T of the weak component. For the four corner points, which mark the extreme combinations of T and n_n, the corresponding $\sigma N(A)$ curves are plotted in Fig. 9 together with the empirical σN values of the s-dominated nuclides in the region of interest.

The present limits on temperature and neutron density for the weak component are compatible with those of the main component (dashed lines in Fig. 8). This is also demonstrated by a $\sigma N(A)$ fit over the whole mass range $56 < A < 210$, which uses identical temperatures and neutron densities for both weak and main component (Fig. 10). It may therefore be concluded that both s processes occured at similar stellar sites.

The present result supports the idea that the classical approach can be a useful tool for deriving constraints on the physical conditions during the *real* s process in stars. It is to be noted that these constraints are independent of the various stellar s-process models,[16,17] but only based on observed abundances and nuclear physics parameters. In this context, an important uncertainty has been removed, leading to an even more consistent picture within the purely phenomenological classical s process. However, the persisting uncertainties—in the classical approach as well as in the stellar models—are still too large to draw final conclusions on the true nature of s-process nucleosynthesis.

Note added in proof. We have decided to present, in Table V, some decisive quantities more explicitly than those given in Fig. 7.

ACKNOWLEDGMENTS

The success of this experiment depended essentially on the excellent technical assistance of G. Rupp, who was also responsible for the production of the carbon disks. Furthermore, we like to thank A. Hanser and B. Feurer for the mass separation of ^{78}Se. Mrs. Kuhn and Mr. Hütsch (Ringsdorff Werke) supplied us with carefully recleaned samples. We appreciate the help of D. Heck and W. Rottmann (KfK), Mr. Gasper (DKFZ, Heidelberg), and of our local contacts at Grenoble, Mr. Borrel, Mr. Robert, and K. Schreckenbach. We thank G. Schatz, who read the manuscript carefully and made us aware of a reference, which improved the accuracy of the present result.

[1]G. Walter, H. Beer, F. Käppeler, and R.-D. Penzhorn, Astron. Astrophys. **155**, 247 (1986).

[2]G. Walter, H. Beer, F. Käppeler, G. Reffo, and F. Fabbri, Astron. Astrophys. **167**, 186 (1986).

[3]K. Takahashi and K. Yokoi, At. Data Nucl. Data Tables **36**, 375 (1987).

[4]K. Cosner and J. W. Truran, Astrophys. Space Sci. **78**, 85 (1981).

[5]H. J. Conrad, Ph.D. thesis, University of Heidelberg, 1976.

[6]J. van Klinken, S. J. Feenstra, and G. Dumont, Nucl. Instrum. Meth. **151**, 433 (1978).

[7]H. Behrens and J. Jänecke, *Numerical Tables for Beta-decay and Electron Capture*, Vol. 4 of Landolt-Börnstein New Series, edited by H. Schopper (Springer-Verlag, Berlin, 1969), Part b.

[8]C. M. Lederer and V. S. Shirley, *Table of Isotopes*, 7th ed. (Wiley, New York, 1978).

[9]R.-D. von Dincklage and J. Gerl, Nucl. Instrum. Meth. A **235**, 198 (1985).

[10]A. H. Wapstra and G. Audi, Nucl. Phys. A **432**, 1 (1985).

[11]H. Beer, G. Walter, R. L. Macklin, and P. J. Patchett, Phys. Rev. C **30**, 464 (1984).

[12]Z. Y. Bao and F. Käppeler, At. Data Nucl. Data Tables **36**, 411 (1987).

[13]W. Ratynski and F. Käppeler, Phys. Rev. C **37**, 595 (1988).
[14]H. Beer (private communication).
[15]H. Beer, Kernforschungszentrum Karlsruhe internal report, 1985.
[16]I. Iben, Jr., and A. Renzini, Ann. Rev. Astron. Astrophys. **21**, 271 (1983).
[17]N. Prantzos, M. Arnould, and J.-P. Arcoragi, Astrophys. J. **315**, 209 (1987).

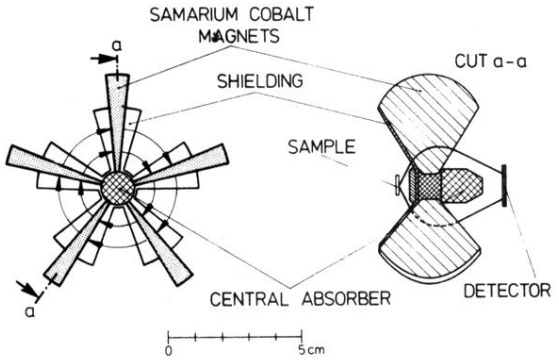

FIG. 2. Mini-orange spectrometer setup for suppression of conversion electrons below 96 keV. Idealized trajectories for electron energies of ~ 140 keV are indicated in the right part of the figure.